Bull Volcanol (2012) 74:1667–1681
DOI 10.1007/s00445-012-0622-0

RESEARCH ARTICLE

Internal flow structures in columnar jointed basalt from Hrepphólar, Iceland: II. Magnetic anisotropy and rock magnetic properties

Bjarne S. G. Almqvist · Sonja A. Bosshard · Ann M. Hirt · Hannes B. Mattsson · György Hetényi

Received: 21 September 2011 / Accepted: 15 May 2012 / Published online: 20 June 2012

Abstract The anisotropy of magnetic susceptibility (AMS) and rock magnetic properties were measured on specimens from a basalt plate that was cut from a vertical section of a basalt column from Hrepphólar, Iceland. Macroscopic structures are clearly distinguishable in the plate, including banding inferred to represent viscous fingering parallel to the vertical axis of the column. Rock magnetic experiments indicate that the dominant ferromagnetic (sensu lato) mineral is titanomagnetite, $Fe_{3-x}Ti_xO_4$, with a Ti-composition of x=~0.6. Magnetic properties are related to the position within the plate and reveal a dominant volume fraction of single domain titanomagnetite in the center of the basalt column, with multidomain titanomagnetite away from the center. The AMS determined by low-field measurements shows an inconclusive relationship with the visual structures, which arises from variation of the grain size (i.e., single domain versus multidomain) across the column. In contrast, the AMS measured with a high-field torsion magnetometer avoids the complication of magnetic domain state, as is demonstrated in this contribution, and additionally allows for the separation of ferrimagnetic from paramagnetic sub-fabrics. Both sub-fabrics display a clear relationship with the macroscopic structures and support the hypothesis that vertical flow of melt took place during development of the Hrepphólar columnar basalt. Maximum susceptibility axes of the ferrimagnetic sub-fabric are grouped near the vertical axis of the column. The paramagnetic sub-fabric varies systematically across the column in coincidence with internal structure. The shape of the magnetic susceptibility ellipsoid varies across the basalt column, showing an increasingly prolate fabric toward its center.

Keywords Magnetic anisotropy · Columnar jointed basalt · Inverse fabric · Ferrimagnetic · Titanomagnetite · Flow structure · Iceland · Hrepphóllar

Editorial responsibility: A. Gudmundsson

Electronic supplementary material The online version of this article (doi:10.1007/s00445-012-0622-0) contains supplementary material, which is available to authorized users.

B. S. G. Almqvist · A. M. Hirt
Institute of Geophysics,
Swiss Federal Institute of Technology (ETH Zürich),
Sonneggstrasse 5,
8092 Zürich, Switzerland

S. A. Bosshard · H. B. Mattsson · G. Hetényi
Institute of Geochemistry and Petrology,
Swiss Federal Institute of Technology (ETH Zürich),
Clausiusstrasse 25,
8092 Zürich, Switzerland

Present Address:
B. S. G. Almqvist (✉)
Geological Institute,
Swiss Federal Institute of Technology (ETH Zürich),
Sonneggstrasse 5,
8092 Zürich, Switzerland
e-mail: bjarne.almqvist@erdw.ethz.ch

Introduction

Preferred orientations of minerals that crystallize during the formation of columnar jointed basalt provide information about the development of internal structures observed in the columns. Titanomagnetite is one of these phases, whose microstructural information (i.e., shape preferred orientation) can be used to help infer when and how crystallization of titanomagnetite takes place inside the column during solidification (e.g., Mattsson et al. 2011). A potential tool

for investigating the petrofabric in basalts and detecting preferred orientation of crystals is the measurement of anisotropy of magnetic susceptibility (AMS; see Table 1 for abbrevations), which can be represented geometrically by an ellipsoid, with axes $k_1 \geq k_2 \geq k_3$. Most research on magnetic properties and AMS in columnar jointed basalts was performed during the 1960s and 1970s (Khan 1962; Brown et al. 1964; Symons 1967; Ellwood and Fisk 1977; Ellwood 1979; Urrutia-Fucugauchi 1982). In their early work, Khan (1962) and Brown et al. (1964) interpreted their AMS data as showing no support for convection or vertical flow of magma inside the column during solidification. One of the most detailed studies on magnetic properties of a single basalt column was made by Symons (1967), who observed a distinctive pattern in the magnetic anisotropy but could not relate it to convection within the viscous magma body or to the formation of the column. In subsequent studies, Ellwood and Fisk (1977) and Ellwood (1979) argued that AMS reflects the thermal contractive stresses that act during formation of basalt columns. Similarly, Urrutia-Fucugauchi (1982) also advocated thermal contractive stresses as influencing the AMS. He, however, also indicated that a number of other factors could influence the AMS, such as primary fabric during emplacement of the lava, chemical alteration during weathering, or crystal growth during late stage cooling. As a consequence, a rather unclear picture has formed with regard to the interpretation of the AMS in columnar jointed basalts (cf. Cãnón-Tapia 2004).

Reconstructing flow directions in dikes is recognized as a general problem (Gudmundsson and Marinoni 1999). AMS measurements may offer considerable insight in the direction of flow, but interpretation is not always straightforward. A feature sometimes observed in AMS of dikes and volcanic rocks is that the axis of maximum susceptibility is oriented normal to the flow-plane or foliation plane, in contrast to the more commonly observed magnetic fabric, defined by the maximum susceptibility parallel to the flow, or within the flow plane (cf. Knight and Walker 1988). One

Table 1 Acronyms and abbreviations used in AMS and rock magnetic studies and in this paper

Term (abbreviation)	Brief definition
Anisotropy of magnetic susceptibility (AMS)	The magnetic anisotropy of a rock due to crystallographic and shape preferred orientation of the rock-forming minerals
Bulk susceptibility (k)	A scalar value that represents the magnetization of a rock in the presence of a static applied field that includes the contribution of all rock-forming
	Minerals (diamagnetic, paramagnetic and ferromagnetic), typically defined as $k=(k1+k2+k3)/3$ or $k=(k1\cdot k2\cdot k3)^{1/3}$
Principal axes of susceptibility (k_1, k_2, k_3)	The three semi-axes of the low-field AMS ellipsoid
Principal axes of the deviatoric susceptibility (l_1, l_2, l_3)	The semi-axes describing the high-field AMS susceptibility ellipsoid as it deviates from a sphere
Degree of anisotropy (P)	The size of the magnetic anisotropy, defined as $P = k_1/k_3$ (measured in low field)
Shape factor (T; determined from k_i)	A description of the shape of the susceptibility ellipsoid, ranging from 1 (oblate) to −1 (prolate); calculated from the low-field AMS
Susceptibility difference (Δk)	The size of the magnetic anisotropy, defined as $\Delta k=l_1-l_3$ (measured in high field)
Shape factor (U; determined from l_i)	A description of the shape of the susceptibility ellipsoid, ranging from 1 (oblate) to −1 (prolate); calculated from the high-field AMS
Curie temperature (T_c)	Temperature above which a ferromagnetic mineral loses its ferromagnetic properties and becomes paramagnetic (reversible and mineral specific)
Alternating gradient magnetometer (AGM)	Analytical instrument to measure magnetic hysteresis properties (M_s, M_{rs}, H_c, and H_{cr})
Saturation magnetization (M_s)	The spontaneous magnetization in the presence of a saturating magnetic field
Remanent saturation magnetization (M_{rs})	The magnetic memory after application of a saturating magnetic field
Coercivity (H_c)	The applied reverse field required to reduce M_s to 0
Coercivity of remanence (H_{cr})	The reverse field required to reduce M_{rs} to 0
Interaction field (H_u)	A measure of the strength of magnetostatic interaction, among and within ferromagnetic crystals
First-order reversal curve (FORC)	A method to represent hysteresis data that provides information on the coercivity (H_c) and magnetic interaction among ferromagnetic minerals (H_u)
Single domain (SD)	A ferromagnetic crystal with a single magnetic domain
Psuedo single domain (PSD)	A ferromagnetic crystal with more than one magnetic domain, but whose magnetic properties are similar to SD crystals
Multidomain (MD)	A ferromagnetic crystal with many magnetic domains

of the earliest observations of this phenomenon was made by Khan (1962) in Tertiary basic dikes from Skye. Later, Symons (1967) and Ellwood (1978, 1979) made similar observations in basalt columns and dikes. A magnetic fabric that has its maximum susceptibility normal to the flow-plane has been labeled an "inverse" fabric and care must be taken when interpreting the origin of this type of magnetic fabric (Raposo and Ernesto 1995; Rochette et al. 1999; Hastie et al. 2011). A mixture of inverse and normal magnetic fabrics (composite fabric) was recently observed in dikes from eastern Iceland (Kissel et al. 2010).

Inverse fabrics in dikes and lavas arise for two reasons. One explanation for an inverse fabric relates to the properties of laminar flow, which can align particles so that their long-axes are normal to the direction of flow (e.g., Jeffrey 1922; Khan 1962), or grains crystallize with their long-axes preferentially perpendicular to the isotherms in the magma (e.g., Rochette et al. 1999). An inverse fabric created in this way does not necessarily imply that the axes of maximum (k_1) and minimum (k_3) susceptibility trade places but rather that the k_1-axis is not oriented parallel to the flow direction. An alternative explanation for the observation of inverse fabrics is related to a shape and size effect of ferrimagnetic grains (Fig. 1). Potter and Stephenson (1988) demonstrated that the magnetization of small ferrimagnetic grains (i.e., single domain grain-size), induced in a susceptibility bridge, depends on the orientation of the grain with respect to the inducing field. The susceptibility is lowest along the long-axis of a single-domain grain, because this is energetically the favorable orientation of the magnetic moment and in effect the magnetization is already saturated along this axis. In contrast, the susceptibility will be higher at angles normal to the grain long-axis. In contrast, the highest susceptibility of multidomain ferrimagnetic minerals is along the long-axis of the grain.

In the present study, we examine the AMS in columnar jointed basalt from Hrepphólar, Iceland, in order to relate magnetic fabric to macroscopic structures that are observed in the basalt. The AMS is investigated using both a low-field susceptibility bridge and high-field torsion magnetometer, in order to compare data that are obtained with the two techniques. Rock magnetic experiments are performed to evaluate differences in composition and grain-size of the ferrimagnetic minerals, which occur in zoned areas of the basalt plate. The characterization and interpretation of mineral texture, petrography, and geochemistry from the same sample is described in Bosshard et al. (2012).

Sample

The sample consists of a vertically cut slab, with dimension 30×44×1 cm (Fig. 2) from a column of basalt, from

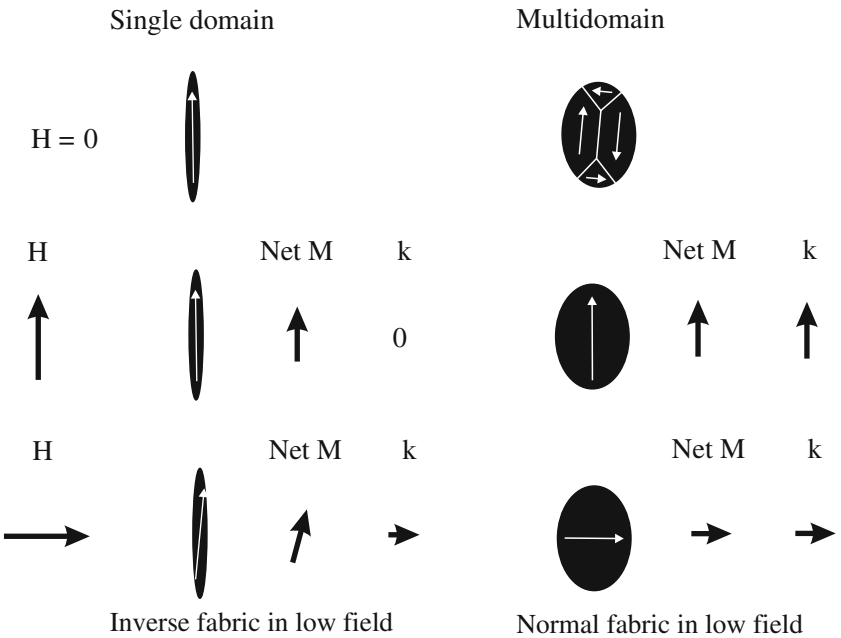

Fig. 1 A simplified sketch that illustrates the concept of inverse magnetic fabric that result from the domain state of ferrimagnetic minerals. All cases consider the application of weak magnetic field (e.g., 300 A/m). The magnitude of the susceptibility of the sample depends on the direction of the applied magnetic field (***H***) and the resultant net magnetization (net ***M***); *k* is the susceptibility. The net magnetization of multidomain grains arises from the magnetic moment produced by the sum of the magnetic domains and the moment inside domain walls (*white lines* separating the domains). During the application of the field, the domain walls are unpinned and the total magnetic moment of the grain is in the direction of the applied field. Domain walls re-nucleate once the field is removed

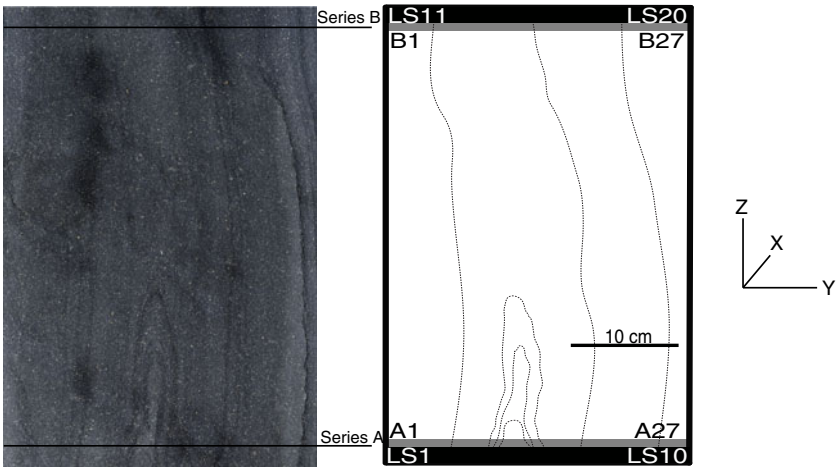

Fig. 2 Photograph and sketch of the basalt plate. The *dark bands* apparent in the photograph are shown as *dashed lines* in the sketch. We interpret the center of the plate as representing the geometric center of the column. The location of the sampled specimens for series A and B are outlined in the sketch. The sections labeled *LS* refer to thin sections discussed by Bosshard et al. (2012). Note that series A specimens were not considered in this study

Hrepphólar, Iceland. It was obtained from the Helgason Ehf rock cutting company and originates from the Hrepphólar lava (Fig. 3). A Cartesian coordinate system is assigned to the sample, where the *Z*-axis corresponds to the vertical axis of the column, and the *X*- and *Y*-axes are in the horizontal plane, perpendicular to the *Z*-axis (Fig. 2). The top of the plate indicates the upward direction in the column. Structures are visible on the polished surface of the basalt plate, which appear as dark bands and cracks surrounded by the lighter, gray, uniform matrix. Cubic specimens with 1 cm sides were cut from the top of the plate in a cross-section profile (series B in Fig. 2). The series contains 27 cubic specimens with 1 cm^3 dimension, on which the magnetic measurements were made. Scanning electron microscope (SEM) images indicate that the grains change shape across the plate, showing euhedral blocky crystals towards the edges of the plate and more elongate grains in the center (Fig. 4). Images were obtained with a JEOL scanning electron microscope.

Methods: AMS and rock magnetism

The bulk susceptibility and low-field AMS were measured with an AGICO KLY-2 Kappabridge. AMS measurements were performed with a standard 15 position measurement scheme (Jelinek 1976), from which it is possible to determine the complete symmetric second rank susceptibility tensor. The eigenvectors and eigenvalues of the tensor represent the orientation and magnitude of the three principal susceptibility axes, with $k_1 \geq k_2 \geq k_3$, which is represented geometrically by an ellipsoid. The degree of anisotropy is given by $P=k_1/k_3$ (Nagata 1961). Shape of the ellipsoid is given by $T=(2\eta_2-\eta_1-\eta_3)/(\eta_1-\eta_3)$, where $\eta_1=ln(k_1)$, $\eta_2=\ln$

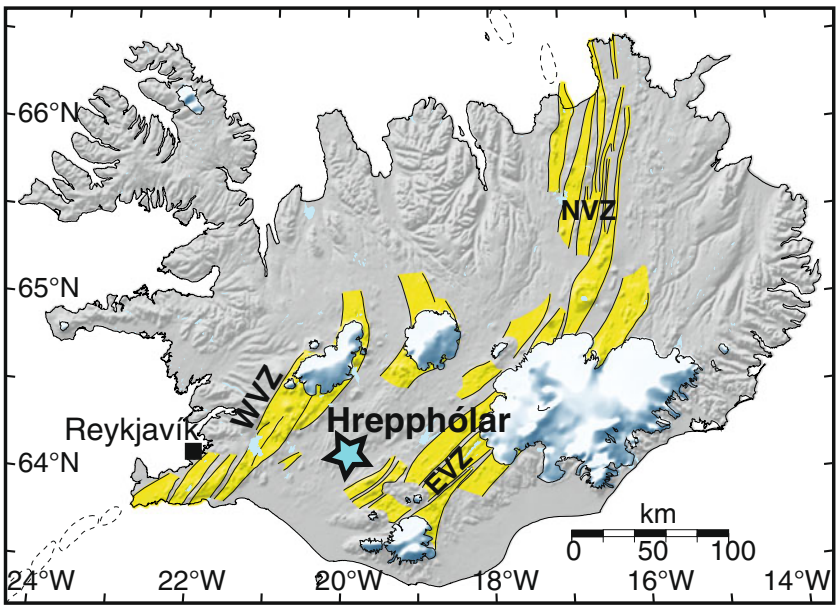

Fig. 3 Map showing the location of Hrepphólar on Iceland; *NVZ* North Volcanic Zone; *EVZ* East Volcanic Zone; *WSZ* West Volcanic Zone

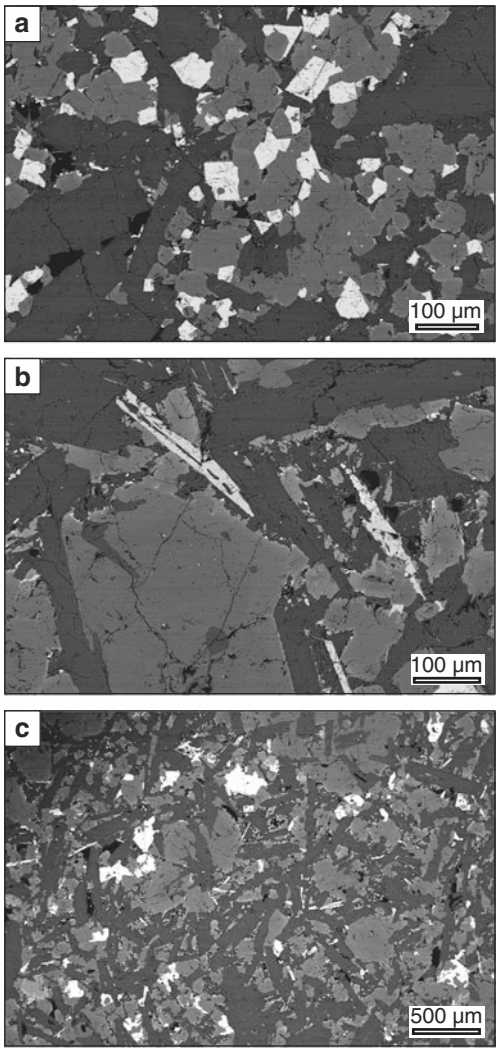

Fig. 4 SEM backscatter electron (*bse*) images showing the shape and size of crystals at **a** the edge and **b** in the center of the basalt plate. The scale is the same in both these images. In **c**, the resolution is lower, providing an overview of a larger area of the crystals in the center of the plate. In all three images, the *bright grey crystals* represent titanomagnetite and illmenite crystals. Evidence for exsolution was not observed in any of the crystals

(k_2) and $\eta_3=\ln(k_3)$ (Jelinek 1981). When $0<T<1$, the ellipsoid has an oblate shape, whereas when $0>T>-1$ the ellipsoid has prolate shape. In specific cases when $T=1$, $T=-1$, and $T=0$, the shape of the susceptibility ellipsoid is respectively rotational oblate, rotational prolate, and neutral. The bulk susceptibility is determined by calculating the arithmetic mean of the low-field principal susceptibility, $k=(k_1+k_2+k_3)/3$.

Additionally a high-field torque magnetometer was used for AMS measurements (Bergmüller et al. 1994). A sample that is suspended between the poles of an electromagnet will experience a magnetic torque, as a consequence of the applied magnetic field. The magnitude of the torque is dependent on the minerals that comprise the sample. A sample composed of paramagnetic minerals that is rotated in a plane containing axes x_1 and x_2 experience a magnetic torque that is proportional to B^2 (the square of the applied field), such that

$$T_3 = \frac{1}{2\mu_0} VB^2[(k_{22} - k_{11})\sin 2\theta + 2k_{12}\cos 2\theta], \quad (1)$$

where V is the volume of the sample, μ_0 is the magnetic permeability of vacuum and θ is the angle between the direction of magnetization and the applied magnetic field. In contrast to a paramagnetic sample, the torque of magnetically saturated ferrimagnetic minerals is controlled by the demagnetizing factor tensor (N_{ij}),

$$T_3 = \frac{1}{2}\mu_0 V_E M_S^2[(N_{22} - N_{11})\sin 2\theta + 2N_{12}\cos 2\theta]. \quad (2)$$

In Eq. 2, M_S is the saturation magnetization of the ferrimagnetic mineral and V_E is the total volume of ferrimagnetic minerals. In the case of magnetite and titanomagnetite, the field necessary to achieve saturation is ~300 mT. Equation 2 was first introduced in Martín-Hernández and Hirt (2001). Note that this equation is expressed somewhat differently than in other studies where magnetic torque has been utilized (e.g., Owens and Bamford 1976; Stevenson et al. 2007). However, there is no essential difference between the equations, and Eq. 2 can be rearranged to match Eq. 2 of Stevenson et al. (2007). One can view the torque as measuring the principal axes of the demagnetization tensor (Owens and Bamford 1976; Stevenson et al. 2007) or the principal axes of susceptibility. We use the latter in this study, because it allows for a more straightforward comparison with principal susceptibility axes of the low-field and paramagnetic AMS. Seven different applied fields were used for the torque measurements, ranging from 700 to 1,500 mT. The magnetic torque was corrected with respect to the specimen holder signal and zero applied field, the latter correcting the magnetic torque signal in the absence of an applied field. Torque measurements provide the deviatoric susceptibility, which expresses the anisotropy in terms of the deviation from a sphere, with principal axes $l_1 \geq l_2 \geq l_3$, where l_3 is always negative and l_2 can be either positive or negative depending on the shape of the susceptibility ellipsoid. It is therefore not possible to use the *P*- and *T*-parameters, which are defined above to describe the low-field AMS. Instead the degree of anisotropy is expressed by Δl, which is the difference between l_1 and l_3 (i.e., $\Delta l = l_1 - l_3$). However, for sake of consistency with susceptibility expressed by k, we will henceforth employ the use of Δk to express the susceptibility difference (which is equivalent with Δl). The shape of the susceptibility ellipsoid is expressed by the parameter U, which is defined as $U=(2l_2-l_1-l_3)/(l_1-l_3)$ (Jelinek 1981). The shape of the susceptibility ellipsoid defined by U is similar to the *T*-parameter, with values ranging from 1 to −1. Separation of the AMS due to paramagnetic and ferrimagnetic (s.s.) minerals was done using the procedure of Martín-Hernández and Hirt

(2001). Examples of torque measurements for two specimens (B4 and B18) used in this study are shown in Fig. 5.

Magnetic properties measurements include hysteresis, first-order reversal curves (FORC), and susceptibility versus temperature (thermomagnetic curves) for selected specimens. Hysteresis loops were performed with an alternating gradient magnetometer (AGM, Princeton Measurements Corporation) on small pieces (mass between 22 and 89 mg) from each specimen in the B-series, which allows determination of the saturation magnetization (M_s), saturation remanent magnetization (M_{rs}), and the coercivity (H_c; Fig. 6). The coercivity of remanence (H_{cr}) was determined from DC demagnetization curves that were made in conjunction with the hysteresis loops and represent the magnetic field necessary to reduce M_{rs} to zero. FORC were measured for selected pieces from the B-series using the AGM. FORC analysis provides information on the distribution of coercivity (H_c) and the interaction field (H_u) in the sample, where the latter is a measure of the strength of magnetostatic interaction (i.e., indicative of the magnetic domain state and the interaction among magnetic particles; Pike et al. 1999). Temperature-dependent susceptibility was measured using the AGICO KLY-2, outfitted with a CS-2 oven.

Results

Anisotropy of magnetic susceptibility

Low-field AMS

Specimens across the column typically display weak magnetic anisotropy, but with consistent orientation of principal axes (Fig. 7a). The k_1-axes are either (1) oriented along the vertical axis of the column, (2) oriented perpendicular to the vertical

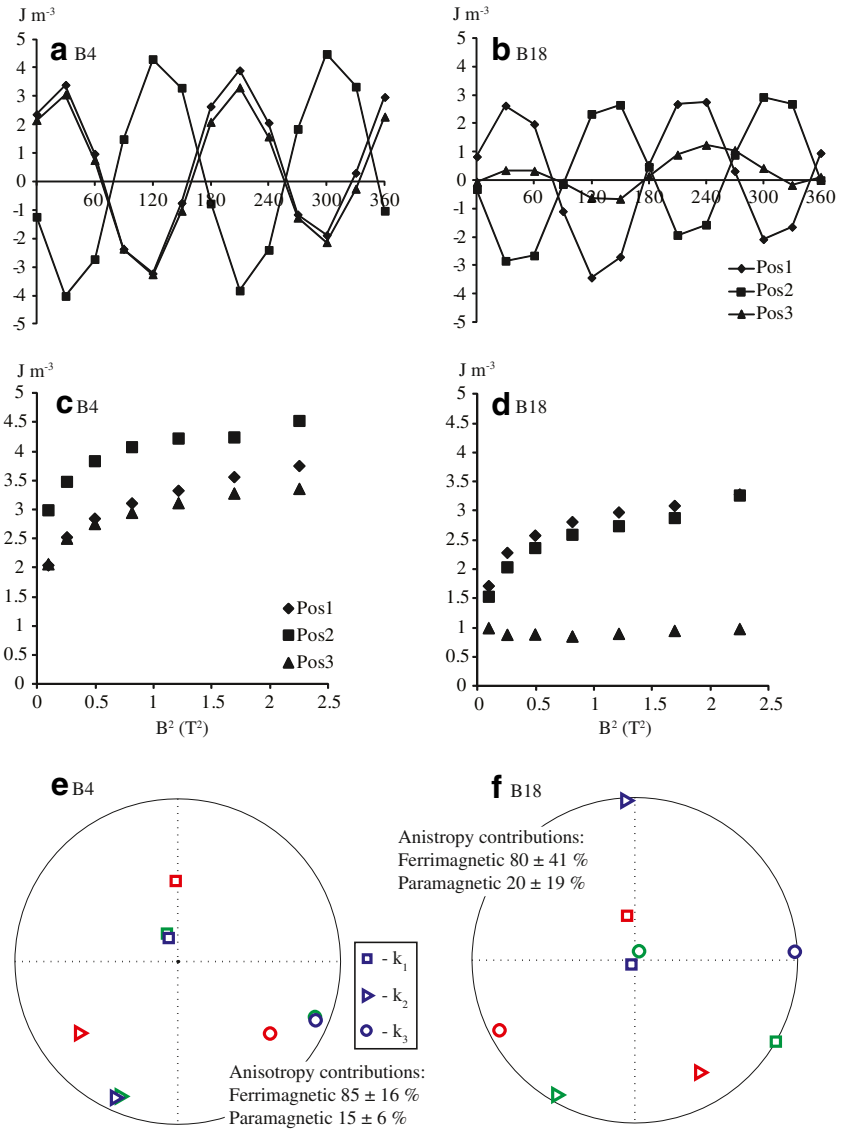

Fig. 5 **a**, **b** The measured torque in three planes, **c**, **d** torque as a function of the field (*squared*), which illustrates the ferrimagnetic versus paramagnetic contribution to anisotropy, and **e**, **f** orientation of principal axes of susceptibility, of low-field (*green*), paramagnetic (*red*), and ferrimagnetic (*blue*) components. *Squares* represent k_1-axes, *triangles* are k_2-axes, and *circles* are k_3-axes. The percentage of paramagnetic and ferrimagnetic contributions are shown

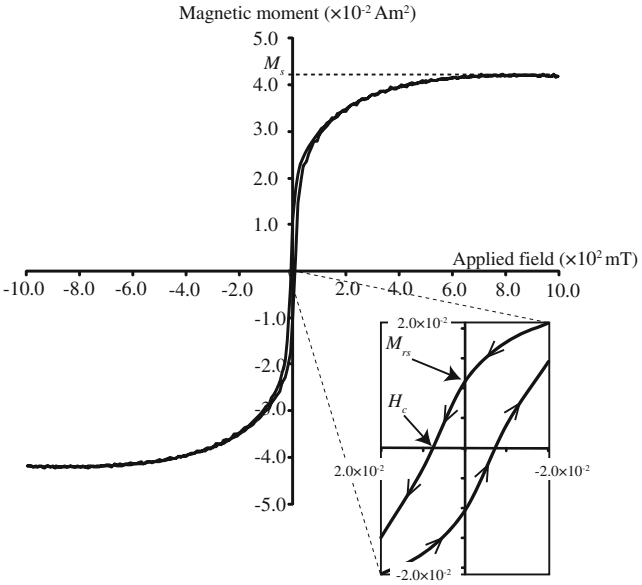

Fig. 6 Hysteresis loop that has been corrected for the high-field paramagnetic susceptibility for specimen B12. The measurement for saturation magnetization (M_s) is indicated by the *dashed line* intersecting the *y*-axis. Similarly, the positions for measurements of the saturation remanent magnetization (M_{rs}) and coercivity (H_c) are shown in the *enlarged section in the lower right side* of the diagram

axis, or (3) in the case of several specimens, oriented at oblique angles with respect to the column. Minimum principal axes are oriented in a similar fashion as k_1, with k_3 either sub-parallel to the long-axis of the column, perpendicular to the vertical axis, or at an intermediate angle (Fig. 7a). Based on the different orientations observed for the principal axes, a scheme has been devised to place specimens in groups of normal, mixed, or inverse fabric. A normal fabric is defined as specimens having their k_1-axis within 20° of the vertical axis of the basalt column (i.e., *Z*-axis of the equal area net); the mixed or intermediate fabric is defined as specimens having their k_1 axis at an angle between 20° and 70° to the vertical axis of the column; the inverse fabric is defined as specimens having angles >70° to the vertical axis of the column and k_3-axes within 20° of the column long-axis. Specimens that show an inverse fabric were sampled mainly from the center of the column, whereas specimens that show normal and mixed fabrics were taken away from the center of the column. The degree of anisotropy (*P*) is low, below 1.10, but increases as a function of bulk susceptibility. The low-field AMS data are provided in the Electronic supplementary material.

High-field AMS

High-field magnetic torque results are shown in Fig. 7b and c, for the separated ferrimagnetic and paramagnetic fabrics, respectively (data are provided in the Electronic supplementary material). The bulk of the anisotropy (>70 %) is controlled by ferrimagnetic minerals, and the ferrimagnetic k_1-axes are sub-parallel to the vertical axis of the column for all specimens, i.e., along the vertical axis, in contrast to the low-field AMS. Data shown in Figs. 7b and 7c are divided into two groups based on their low-field AMS fabrics (i.e., inverse and normal/mixed magnetic fabrics). Specimens that display normal and mixed fabrics are highly clustered with k_1-axes plunging steeply to the northeast. In comparison, the k_2 and k_3 axes are distributed in a girdle in the horizontal plane for specimens with inverse character. The paramagnetic anisotropy represents less than 30 % of the total anisotropy, but a clear fabric is identified (Fig. 7c). Overall, paramagnetic k_1- and k_2-axes form a girdle distribution whose plane intersects the vertical axis of the column, and k_3-axes cluster sub-horizontally to the W–WSW.

The variation in the degree of anisotropy across the plate is shown in Fig. 8 for both paramagnetic and ferrimagnetic sub-fabrics. The trend in the data is similar for the two sub-fabrics, although the degree of anisotropy, represented by Δk, is significantly higher for the ferrimagnetic anisotropy. A general feature of the data is higher values for *k* in the center of the plate, compared with the edges of the plate. Also, the shape changes from oblate or near neutral at the edges of the plate towards the prolate field in the center of the plate.

Rock magnetic properties

Bulk susceptibility and susceptibility versus temperature

Bulk susceptibility (*k*) varies according to the position of the specimen along the sampled profile and ranges from 9.46 to 67.15×10^{-3} SI in series B (Fig. 9a). Values for *k* indicate that the signal is due dominantly to ferrimagnetic minerals. Higher susceptibility coincides with the dark bands observed in the plate.

The susceptibility versus temperature was measured for five selected specimens, from the B-series (B4, B8, B9, B18, and B22; Fig. 10). Each specimen was initially heated to 700 °C in air, using a heating rate of 5 °C/min, followed by gradual cooling back to or near room temperature at a rate of 5 °C/min, while measurements were made continuously. The thermomagnetic curves indicate a Curie temperature around 200 °C as seen from the change in slope. A further change in the heating curve is found around 580 °C, which is indicative of stoichiometric magnetite. The rapid decrease in susceptibility between 50 °C and 200 °C indicates the presence of titanomagnetite (Nagata 1961; Vahle and Kontny 2005). This drop is substantially larger than changes in susceptibility occurring at other temperatures, which means that titanomagnetite is by volume the dominant ferrimagnetic phase. During cooling, there is a notable increase in susceptibility at 580 °C, compared with the drop in susceptibility around the same temperature during heating, indicating that a pure magnetite has formed during heating. The shape of the cooling curve presents another interesting feature when comparing specimens within the

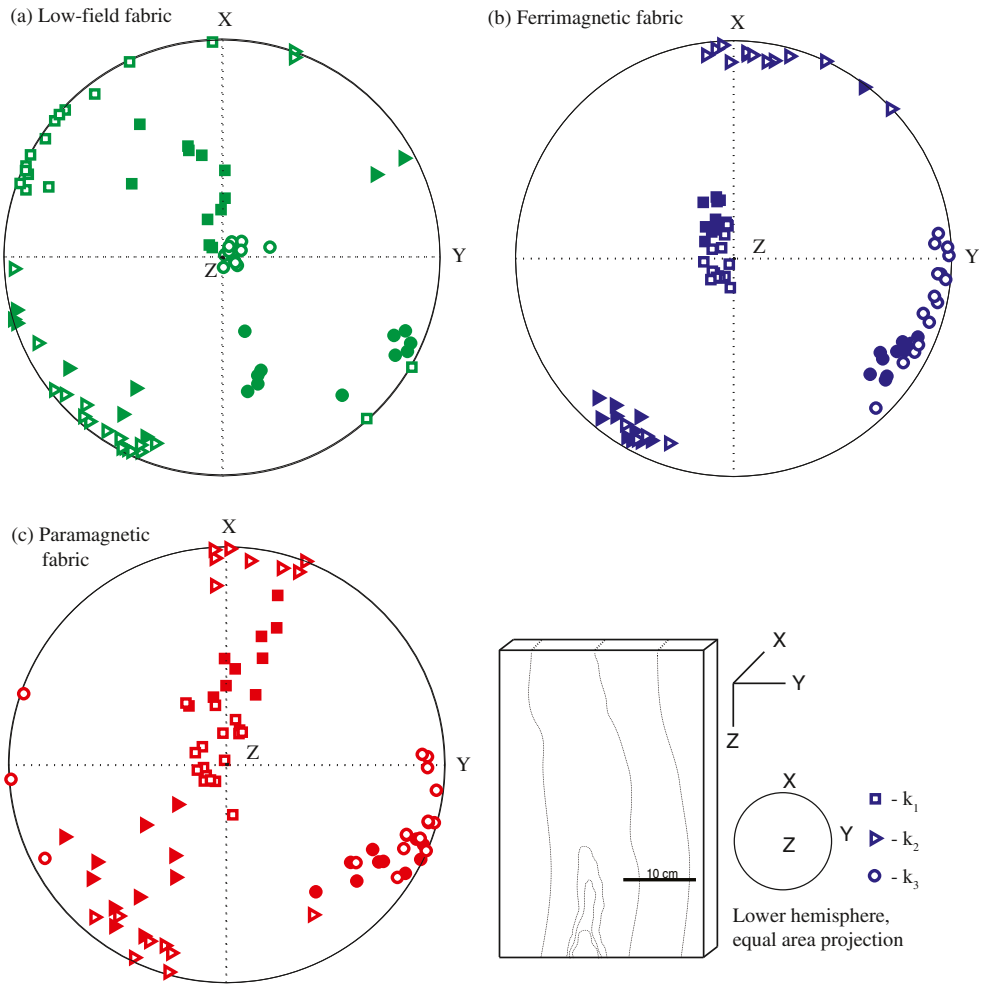

Fig. 7 *Lower hemisphere*, equal area projections presenting the AMS for the B-series specimens performed in **a** low-field. **b**, **c** Represent the separated ferrimagnetic and paramagnetic fabrics, respectively, obtained from measurements with the high-field torsion magnetometer. *Squares* represent k_1-axes, *triangles* are k_2-axes, and *circles* are k_3-axes. *Filled symbols* are specimens that display normal and mixed fabrics in low-field, whereas *open symbols* are specimens with inverse fabric in low-field

sample series. Specimens B8, B9, and B18 show a continuous increase in susceptibility along the entire cooling curve, whereas specimen B4 display a plateau between 450 °C and 150 °C, with no significant increase in susceptibility over this temperature interval.

Hysteresis and first-order reversal curves (FORC)

Saturation magnetization (M_s), saturation remanent magnetization (M_{rs}), coercivity (H_c), and the coercivity of remanence (H_{cr}), determined from the hysteresis loops are correlated with the structures observed in the plate (Fig. 9b, c; Table 2). The ratio of M_{rs}/M_s is low in the part where the darker banding is apparent and higher between the bands. Variation in H_{cr}/H_c is also clear, where the ratio is high in the area of the dark bands and considerably lower between the bands. The H_{cr}/H_c and M_{rs}/M_s for specimens originating from the dark bands suggest overall coarser grain-size of the titanomagnetite, compared with H_{cr}/H_c and M_{rs}/M_s in the surrounding matrix, where the grain-size is on average smaller.

FORCs were measured for specimens B4, B9, B18, and B22, which represent two specimens with high bulk susceptibility (B4 and B22) and two specimens with comparatively low bulk susceptibility (B9 and B18). Processing of the FORCs was done with the locally weighted regression smoothing technique (Harrison and Feinberg 2008), using a smoothing factor of 3; results of the processed data are shown in Fig. 11. Specimens B4 and B22 display similar characteristics, with the peak of the H_c occurring at the origin. Specimens B9 and B18 have the peak concentration of H_c at values between 3 and 5 mT. The interaction field (H_u) is similar for all specimens, but B4 has a broader distribution of H_u. Results from the FORC measurements indicate that, on average, the titanomagnetite grain-size is larger for specimens B4 and B22 compared with the relative smaller grain-size of B9 and B18.

Discussion

Composition of titanomagnetite and magnetic granulometry

The specimens show a Curie temperature of 200 °C or below, which indicates that the bulk ferromagnetic (s.l.) mineral is titanomagnetite with a composition $Fe_{3-x}Ti_xO_4$,

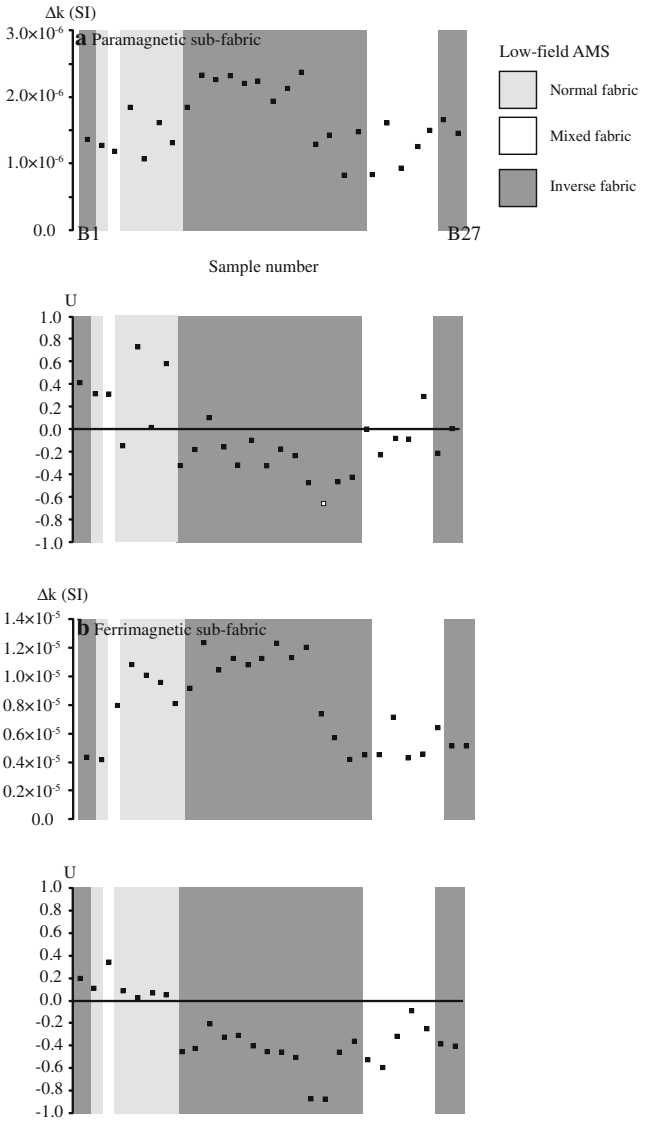

Fig. 8 The susceptibility difference (Δk) and shape-parameter (U), as a function of specimen number in the cross-section, for **a** the paramagnetic sub-fabric and **b** the ferrimagnetic sub-fabric. The *shaded* fields in the background are used to indicate samples that display normal anisotropy (*light grey*), mixed anisotropy (*white*), and inverse anisotropy (*dark grey*)

where $x \geq 0.6$ (e.g., Nagata 1961; Rahman and Parry 1978). The inferred composition, which is based on the Curie temperature, is supported by the compositional data for grains of titanomagnetite obtained with the electron microprobe (Bosshard et al. 2012). Production of stoichiometric magnetite, which is evident from the increase in susceptibility during cooling, arises either at the expense of titanomagnetite (i.e., producing exsolution end members of Ti-rich and Ti-poor oxides), or through the creation of magnetite from alteration of other minerals present in the basalt (e.g., olivine). The fact that it is not possible to see the low Curie temperature subsequent to heating suggests that the original $Fe_{2.4}Ti_{0.6}O_4$ has exsolved into Fe_3O_4 and $FeTiO_3$.

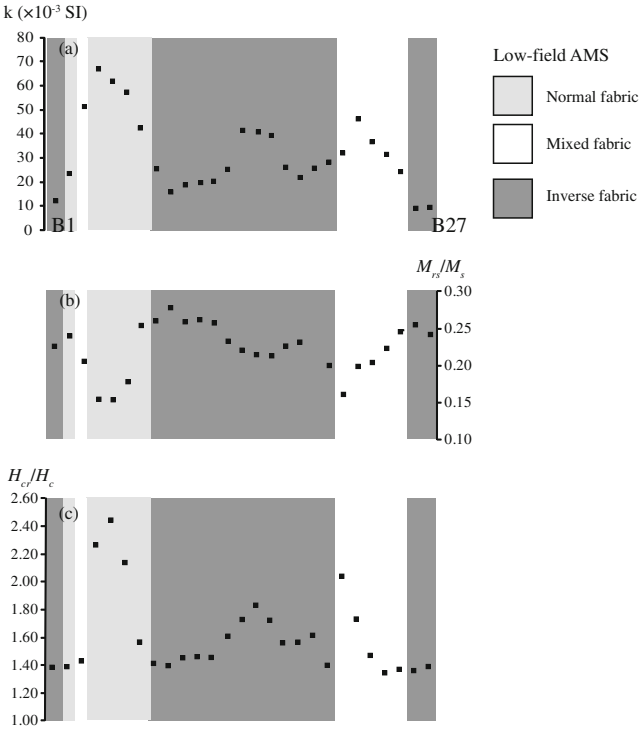

Fig. 9 **a** Bulk susceptibility, **b** M_{rs}/M_s and the **c** H_{cr}/H_c as a function of position across the basalt plate

The rock magnetic properties and AMS change according to the macroscopic structures observed in the basalt plate. Bulk susceptibility is high where the dark bands occur ($>60\times10^{-3}$ SI), whereas it is significantly lower in the brighter part between the bands. The ratios of M_{rs}/M_s and H_{cr}/H_c suggest that this is not only a matter of concentration of ferrimagnetic grains but rather a consequence of different grain-size of the titanomagnetite in the bands versus between the bands. Multidomain (MD) grains have higher bulk susceptibility than single domain (SD) grains. Grain-size difference is also indicated by the FORC measurements, which suggests that the volume fraction of MD grains present in the dark bands is higher compared with that between the bands, where the bulk magnetic properties are dominated by SD grains. The concentration of titanomagnetite is a few percent higher in the dark bands, which yields higher bulk susceptibility. Hydrothermal alteration was ruled out as a factor responsible for creating dark versus light bands, because no hydrated phases were encountered (see Bosshard et al. 2012).

Plotting the fraction of H_{cr}/H_c against the M_{rs}/M_s (Day et al. 1977) provides some insight on the grain-size of the titanomagnetite (Fig. 12). The data are displayed using different shading, based on their low-field AMS characteristics (section "Low-field AMS"). Specimens that display inverse or mixed fabrics have high M_{rs}/M_s and low H_{cr}/H_c, in comparison with specimens that showed normal fabrics, for which M_{rs}/M_s is lower and H_{cr}/H_c is higher. There is a

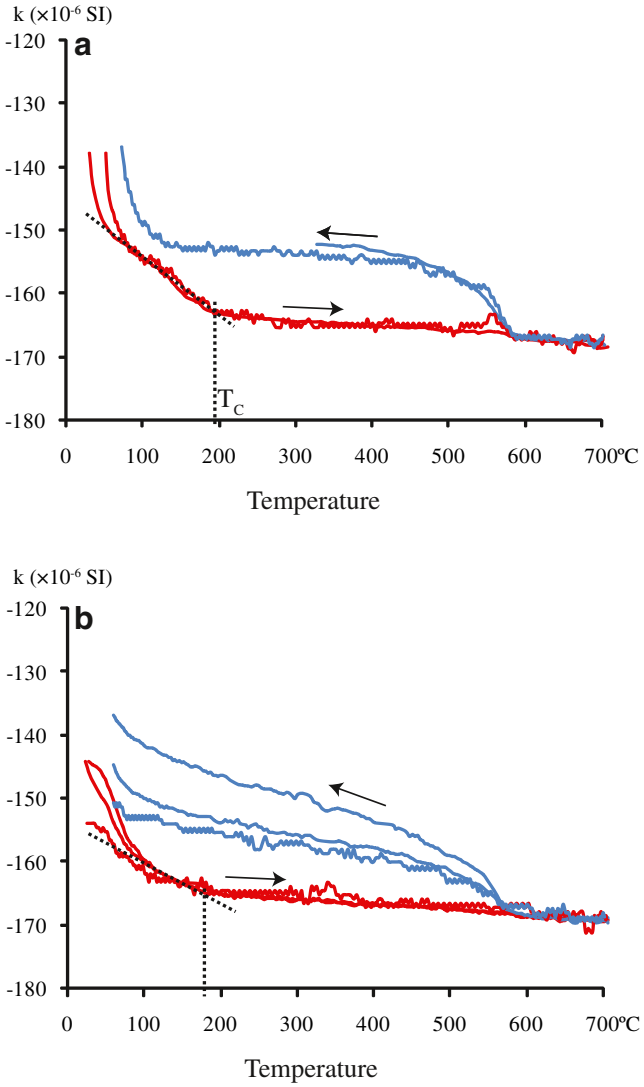

Fig. 10 Susceptibility as a function of temperature for **a** specimens B4 and B22 and **b** specimens B8, B9, and B18. The *red curves* correspond to heating from room temperature up to 700 °C, whereas the *blue curves* represent cooling from 700 °C, back to room temperature. Note that bulk susceptibility (k) has not been corrected for the contribution of the holder signal to the measurements and only the relative susceptibility changes are shown; T_C is Curie temperature

gradual coarsening of the titanomagnetite from specimens with inverse to mixed to normal magnetic fabric with a grain-size distribution spanning across the SD to MD threshold. An inverse magnetic fabric is expected from low-field AMS measurements when the volume of SD titanomagnetite is larger than the volume of MD grains and given the condition that SD grains exhibit shape anisotropy. The critical SD to MD grain-size transition is thought to occur at about 1–2 μm (Dunlop 2002a, b) and is an order of magnitude larger compared with stoichiometric magnetite. It is notably difficult to predict the volume fractions of SD and MD titanomagnetite (Dunlop 2002a), and therefore no attempt has been made to estimate the volume fraction for each grain-size fraction. Hartstra (1982) and O'Donovan et al. (1986) published hysteresis values for titanomagnetite with x~0.6, with values of M_{rs}/M_s ranging from ~0.1 to ~0.3 and H_{cr}/H_c from ~2 to ~4.5. Hrepphólar titanomagnetite show similar values, although H_{cr}/H_c (Fig. 8) is somewhat lower compared with these earlier studies and likely arise from large variations observed in grain-size (from a few millimeters to a less than 1 μm; Fig. 4). An increasing amount of SD titanomagnetite would shift the H_{cr}/H_c toward lower values, as is noted for example by Hartstra (1982). Note that fine-scaled exsolution (~1 μm) was not discovered by electron microscopy, and no evidence for alteration of the basalt or partial maghemitization of the titanomagnetite was found. In addition, fine-scaled exsolution is inconsistent with the Curie temperature that is observed for the Hrepphólar samples, below 200 °C. In a recent study, Kissel et al. (2010) showed similar magnetomineralogical properties for dikes from eastern Iceland, although their Ti-content was bimodal, with either Ti-poor titanomagnetite (x~0.15) or Ti-rich titanomagnetite (x~0.6) and hysteresis parameters reported in their study are very similar to what we have observed for the Hrepphólar basalt. In addition, they observed similar characteristics for the low-field AMS.

Origin of the magnetic fabric in the Hrepphólar basalt

The low-field AMS indicate that either k_1 or k_3 axes preferentially align parallel to the vertical axis of the column in different samples along the profile. The former case occurs in specimens from the dark bands, whereas the latter case occurs for specimens between the dark bands. In contrast, the high-field AMS always show k_1-axes parallel to the long-axis of the column. This discrepancy arises because of the "inverse" anisotropy effect produced by measurements using the low-field susceptibility. The inverse anisotropy, observed from low-field measurements, can be explained by the presence of non-equidimensional SD titanomagnetite, whose susceptibility is smallest along their grain long-axes and largest normal to the grain long-axes (cf. Potter and Stephenson 1988; Rochette et al. 1991, 1999). Magnetic torque measurements reveal k_1-axes oriented parallel to the column axis, indicating that torque measurements do not give rise to the inverse anisotropy seen by low-field measurements.

Further evidence for a domain-size origin to the inverse anisotropy are based on comparisons of rock magnetic experiments and the AMS data, as well as SEM images demonstrating needle-like crystals in the center of the column (Fig. 4b, c). Judging from the hysteresis parameters (Table 2) and the low-field magnetic fabrics, it appears that MD and SD grains are present in concentrations such that their magnetic properties carry nearly equal weight. Since magnetic torque measurements of ferromagnetic grains do

Table 2 Hysteresis parameters and magnetic fabric for the sample B-series

Specimen	Mass (g)	M_s (Am^2)	M_{rs} (Am^2)	H_c (mT)	H_{cr} (mT)	M_{rs}/M_s	H_{cr}/H_c	Magnetic fabric
B1	0.0890	4.23E-01	9.62E-02	8.32	11.53	0.23	1.39	I
B2	0.0318	3.59E-01	8.66E-02	7.68	10.72	0.24	1.39	N
B3	0.0574	4.44E-01	9.12E-02	6.77	9.71	0.21	1.43	M
B4	0.0798	8.10E-01	1.25E-01	4.14	9.37	0.15	2.27	N
B5	0.0402	9.40E-01	1.45E-01	4.41	10.83	0.15	2.46	N
B6	0.0642	8.50E-01	1.51E-01	5.38	11.50	0.18	2.14	N
B7	0.0493	6.10E-01	1.55E-01	7.67	12.01	0.25	1.57	N
B8	0.0630	5.68E-01	1.48E-01	7.55	10.68	0.26	1.41	I
B9	0.0222	5.58E-01	1.55E-01	6.85	9.57	0.28	1.40	I
B10	0.0668	7.73E-01	2.00E-01	7.28	10.60	0.26	1.46	I
B11	0.0571	7.73E-01	2.03E-01	7.57	11.06	0.26	1.46	I
B12	0.0576	7.26E-01	1.87E-01	7.52	10.95	0.26	1.46	I
B13	0.0569	8.13E-01	1.89E-01	6.72	10.70	0.23	1.59	I
B14	0.0659	9.22E-01	2.03E-01	6.35	10.93	0.22	1.72	I
B15	0.0422	9.74E-01	2.09E-01	5.94	10.88	0.21	1.83	I
B16	0.0606	9.58E-01	2.05E-01	6.03	10.43	0.21	1.73	I
B17	0.0672	8.18E-01	1.86E-01	6.36	9.93	0.23	1.56	I
B18	0.0575	7.37E-01	1.71E-01	5.79	9.05	0.23	1.56	I
B19	0.0763	6.39E-01	1.39E-01	5.92	9.57	0.22	1.62	I
B20	0.0565	6.38E-01	1.28E-01	5.59	7.81	0.20	1.40	I
B21	0.0556	8.59E-01	1.38E-01	4.26	8.72	0.16	2.05	M
B22	0.0660	5.66E-01	1.13E-01	4.88	8.55	0.20	1.75	M
B23	0.0796	5.63E-01	1.15E-01	6.55	9.63	0.20	1.47	M
B24	0.0626	4.53E-01	1.01E-01	6.88	9.25	0.22	1.35	M
B25	0.0454	3.39E-01	8.36E-02	7.59	10.41	0.25	1.37	M
B26	0.0664	3.63E-01	9.29E-02	8.48	11.54	0.26	1.36	I
B27	0.0338	3.48E-01	8.45E-02	7.85	10.89	0.24	1.39	I

N normal, *M* mixed, *I* inverse

not operate on the premises of a weak inducing field as for low-field AMS, but rather on the demagnetization factor, the inverse anisotropy effect of elongate SD grains does not occur. Comparison of AMS results from the two techniques can therefore serve to effectively identify the source of the inverse fabric, which in the Hrepphólar basalt is due to SD titanomagnetite and not due to imbrication or rotation of grain long-axes normal to the direction of flow.

AMS in columnar basalt: a late-stage cooling fabric indicator

The visible dark bands at Hrepphólar suggest that vertical displacement of material took place during or subsequent to thermal contraction and formation of the columnar joints, which produced a preferred orientation of crystals in the column (Mattsson et al. 2011). Titanomagnetite is of particular interest in this case, as it crystallizes late in the cooling history (Wright and Okamura 1977), and its orientation can thus be used as a measure of the late-stage melt migration in the basalt. Titanomagnetite crystals are aligned with their long axes parallel to the macroscopic structures in the basalt plate. Since columnar jointing has taken place, the AMS data indicate that the magnetic fabric due to titanomagnetite is not related to primary emplacement of the basaltic lava (i.e., a foliation dominated fabric) but rather to the late stages of solidification and column formation resulting in upward central displacement of material inside the columns. The melt migration is controlled by the crack propagation that takes place during columnar jointing, as well as to the volume decrease associated with column-internal crystallization of minerals during late-stage cooling (Mattsson et al. 2011).

Another interesting feature that is observed from the AMS is change in degree of anisotropy and ellipsoid shape across the basalt plate. The results show that the susceptibility ellipsoid becomes increasingly prolate towards the center of the column. Such a trend has also been observed in basalt columns previously by Ellwood and Fisk (1977),

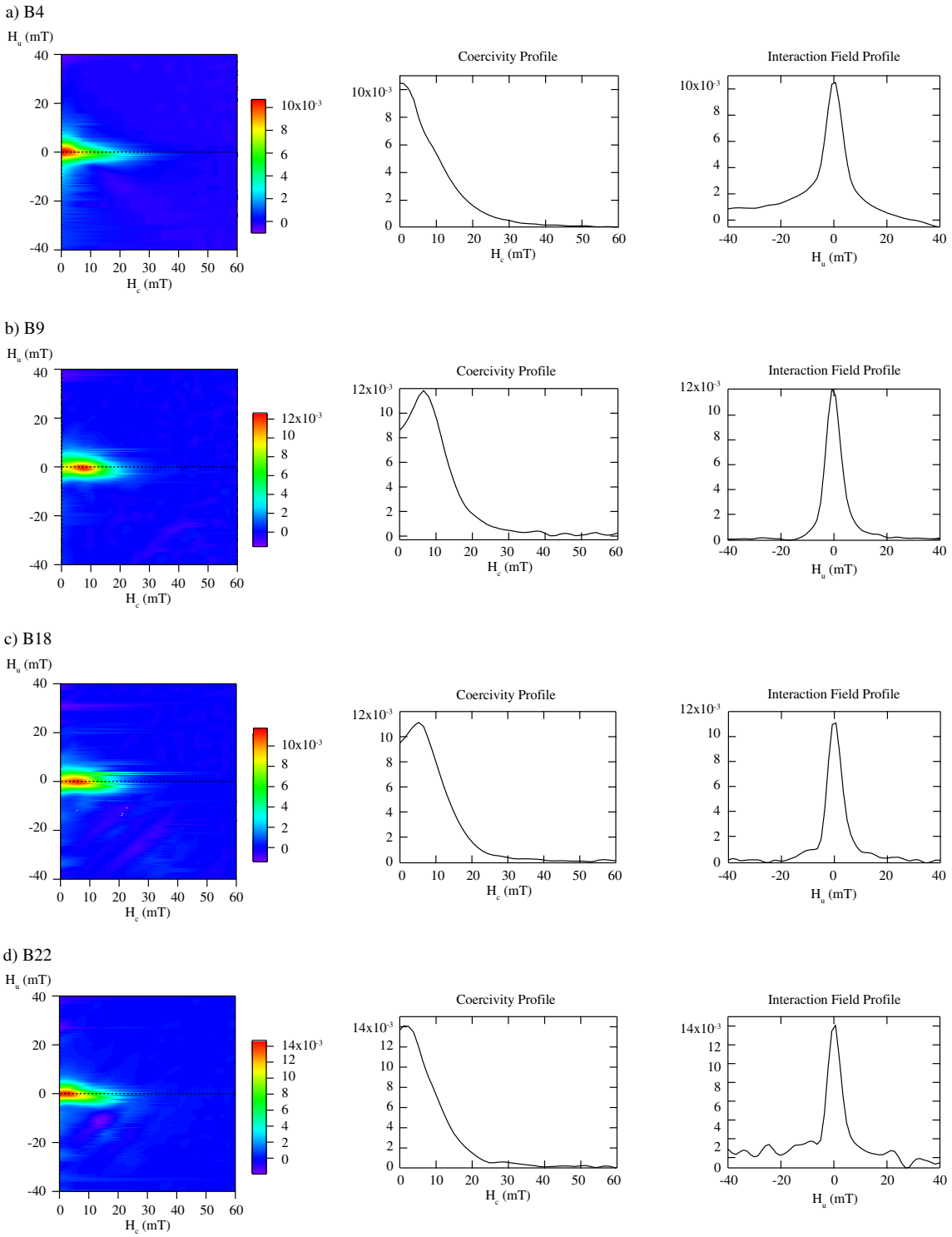

Fig. 11 First-order reversal curve (FORC) diagrams for specimens **a** B4, **b** B9, **c** B18, and **d** B22, showing the distribution of coercivity (H_c) and interaction field (H_u) of ferromagnetic particles in each specimen

and later Urrutia-Fucugauchi (1982). Ellwood and Fisk (1977) suggested that an elongation of the susceptibility ellipsoid existed in areas where the column remained in liquid state for the longest time and that higher temperatures are sustained in the center of the column. This appears to be the case also for the Hrepphólar column (Figs. 2 and 8), which additionally supports the idea that melt migrated during solidification. The degree of anisotropy is highest

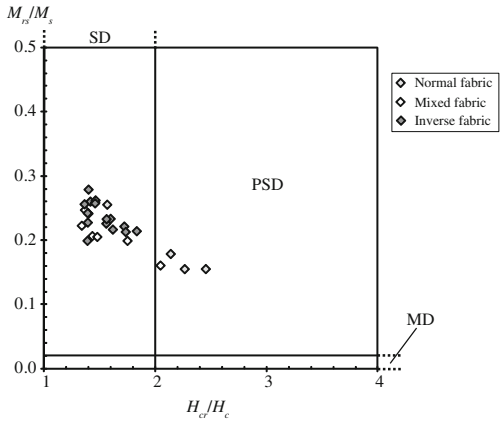

Fig. 12 M_{rs}/M_s plotted against H_{cr}/H_c (Day-plot) for specimens from the B-series. The theoretical single domain (SD), pseudo-single domain (PSD), and multidomain (MD) fields for magnetite are indicated in the diagram (Dunlop 2002a). The data are sub-divided into three categories based in their low-field AMS (as indicated in Table 2 and Fig. 2): *dark grey diamonds* represent specimens that display an inverse fabric, *white diamonds* have a mixed fabric, and *light grey diamonds* display a normal fabric

in the central portion, where solidification occurred last, and the AMS can effectively be used to distinguish the edges of the basalt plate from the geometric center of the plate. However, the variation of the degree of anisotropy is not strictly symmetrical. The changes in shape and degree of the susceptibility ellipsoid also agree well with the microstructural observations from SEM images across the plate. Increasing Δk and a prolate shape anisotropy in the center of the plate can be explained by a higher concentration of elongate or needle-like titanomagnetite crystals, as observed in Fig. 2b and c. Conversely, the AMS is neutral (U~0) at the edges of the plate, which is consistent with more equant-shape crystals identified in the SEM images (Fig. 2a). The AMS therefore reflects different stages and mechanisms operating during solidification.

Gradual rotation of the ferrimagnetic axis of maximum susceptibility is apparent across the plate (Fig. 13). On the left side of the plate, specimens have k_1-axes in the northeast quadrant on the lower-hemisphere equal-area nets, but their orientations gradually migrate toward the southeast quadrant from the left side of the plate toward the center (Fig. 13). The k_1-axes of specimens from the right side of the plate move back to the northeast quadrant of the plate. The change in orientation of k_1-axes indicate that the ferrimagnetic AMS captures the subtle differences in orientation of the titanomagnetite in the plate. These results, in terms of orientation, shape, and degree of AMS, can be interpreted as revealing a detailed history of internal column formation and reflect the vertical migration of melt within the column (c.f. Mattsson et al. 2011). One explanation for the subtle variation in the susceptibility is viscosity differences in the migrating melt, from the outer part of the column towards the center. This difference imposes shear stresses within the column that rotate existing crystals of titanomagnetite and force a preferred orientation on *in situ* crystallized titanomagnetite, which in turn gives rise to the observed AMS. Aspects of the observed AMS pattern are inferred to reflect (1) stresses related to both lateral and vertical contraction of the column (e.g., Ellwood and Fisk 1977; Urrutia-Fucugauchi 1982), (2) formation of microscopic percolation structures or "channels" in the column, whose shapes are

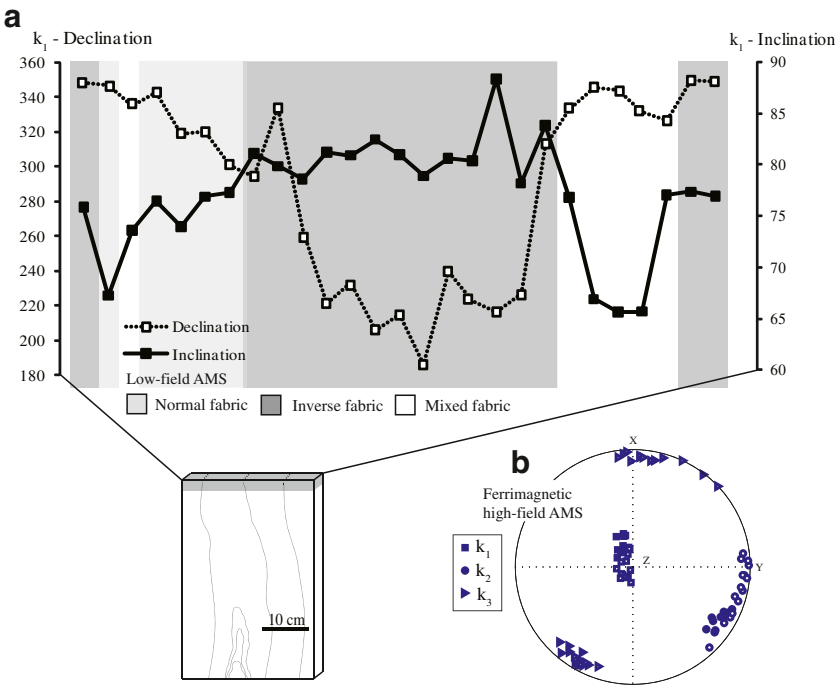

Fig. 13 **a** Orientations of declination and inclination for the k_1-axes of the ferrimagnetic fabric, for specimens across the plate (B-series; see *inset* schematic of basaltic plate). The different types of low-field AMS fabrics are indicated by *light gray* (normal fabric), *white* (mixed fabric), and *dark gray* (inverse fabric). **b** The principal axes of the maximum (*squares*), intermediate (*triangles*), and minimum (*circles*) ferrimagnetic susceptibility. *Filled symbols* are specimens that display normal and mixed fabrics in low-field, whereas *open symbols* are specimens with inverse fabric in low-field

dictated by the earlier crystallized minerals, through which melt is transported (e.g., the formation of plagioclase chain-networks; e.g., Philpotts et al. 1998), and (3) in situ crystallization of titanomagnetite with shape-preferred orientation.

Conclusions

Anisotropy of magnetic susceptibility and magnetic properties have been measured for specimens in a plate originating from columnar jointed basalt, collected from Hrepphólar (Iceland), in order to assist interpretation of macroscopic features observed in the plate. Titanomagnetite, with composition $Fe_{3-x}Ti_xO_4$ where $x \geq 0.6$, is responsible for the magnetic anisotropy as is evident from both measurements in low-field with a KLY-2 Kappabridge and in high field with a torque magnetometer. Whereas the low-field measurements provide results showing both normal and inverse magnetic fabric, the results obtained from the torque magnetometer produce only a normal magnetic fabric, where the latter result is a consequence of the measurement technique. The inverse fabric that is observed from low-field measurements is interpreted as arising from single domain titanomagnetite, rather than imbrication of grains with their long-axes normal to the macroscopic structures of the columnar basalt. Growth of titanomagnetite crystals, the last phase to crystallize during cooling of the columnar basalt, coincided with development of the macroscopic structural features visible in the basalt sample. The orientation of the titanomagnetite grains suggests near-continuous displacement of material in the columns. Subtle variation across the column is apparent in the ferrimagnetic AMS, an effect likely reflecting the physical conditions imposed on the growth of titanomagnetite.

Acknowledgments We thank Carl Stevenson, Sigurdur Steinthorsson, two anonymous reviewers, the associate editor Agust Gudmundsson, and editor James White for helpful reviews that significantly improved the manuscript.

References

Bergmüller F, Bärlocher C, Geyer B, Grieder M, Heller F, Zweifel P (1994) A torque magnetometer for measurements of the high-field anisotropy of rocks and crystals. Meas Sci Technol 5:1466–1470

Bosshard SA, Mattsson HB, Hetényi G (2012) Internal flow structures in columnar jointed basalt from Hrepphólar, Iceland: I. Textural and geochemical characterization. Bull Volcanol. doi:10.1007/s00445-012-0623-z

Brown HC, Khan MA, Stacey FD (1964) A search for flow structure in columnar basalt using magnetic anisotropy measurements. PAGEOPH 57:61–65

Cãnón-Tapia E (2004) Anisotropy of magnetic susceptibility of lava flows and dykes: a historical account. In: Martín-Hernández F, Lüneberg CM, Aubourg C, Jackson M (eds) Magnetic fabric: methods and applications. Geol Soc London Spec Publ 238:205–225

Day R, Fuller M, Schmidt VA (1977) Hysteresis properties of titanomagnetites: grain-size and compositional dependence. Phys Earth Planet Inter 13:260–267

Dunlop DJ (2002a) Theory and application of the Day plot (M_{rs}/M_s versus H_{cr}/H_c), 1, theoretical curves and tests using titanomagnetite data. J Geophys Res 107. doi:10.1029/2001JB000486

Dunlop DJ (2002b) Theory and application of the Day plot (M_{rs}/M_s versus H_{cr}/H_c), 2, application to data for rocks, sediments and soils. J Geophys Res 103. doi:10.1029/2001JB000487

Ellwood BB (1978) Flow and emplacement direction determined for selected basalt bodies using magnetic susceptibility anisotropy measurements. Earth Planet Sci Lett 41:254–264

Ellwood BB (1979) Anisotropy of magnetic susceptibility variations in Icelandic columnar basalts. Earth Planet Sci Lett 42:209–212

Ellwood BB, Fisk MR (1977) Anisotropy of magnetic susceptibility variations in a single Icelandic columnar basalt. Earth Planet Sci Lett 35:116–122

Gudmundsson A, Marinoni LB (1999) Geometry, emplacement, and arrest of dykes. Ann Tectonicæ 13:71–92

Harrison RJ, Feinberg JM (2008) FORCinel: an improved algorithm for calculating first-order reversal curve distributions using locally weighted regression smoothing. Geochem Geophys Geosyst 9. doi:10.1029/2008GC001987

Hartstra RL (1982) Grain-size dependence on initial susceptibility and saturation magnetization-related parameters of four natural magnetites in the PSD-MD range. Geophys J R Astron Soc 71:477–495

Hastie WW, Aubourg C, Watkeys MK (2011) When an 'inverse' fabric is not inverse: an integrated AMS-SPO study in MORB-like dykes. Terra Nova 2:49–55

Jeffrey GB (1922) The motion of ellipsoidal particles immersed in a viscous fluid. Proc R Soc Lond A 102:161–179

Jelinek V (1976) The statistical theory of measuring anisotropy of magnetic susceptibility of rocks and its application. Geophysika, Brno

Jelinek V (1981) Characterization of the magnetic fabric of rocks. Tectonophysics 79:T63–T67

Khan MA (1962) The anisotropy of magnetic susceptibility of some igneous and metamorphic rocks. J Geophys Res 67:2873–2885

Kissel C, Laj C, Sigurdsson H, Guillou H (2010) Emplacement of magma in Eastern Iceland dikes: insights from magnetic fabric and rock magnetic analyses. J Volcanol Geotherm Res 191:79–92

Knight MD, Walker GP (1988) Magma flow directions in dikes of the Koolay complex, Oahu, determined from magnetic fabric studies. J Geophys Res 93:4301–4319

Martín-Hernández F, Hirt AM (2001) Separation of ferrimagnetic and paramagnetic anisotropies using a high-field torsion magnetometer. Tectonophysics 337:209–221

Mattsson HB, Caricchi L, Almqvist BSG, Caddick MJ, Bosshard SA, Hetényi G, Hirt AM (2011) Melt migration in basalt columns driven by crystallization-induced pressure gradients. Nat Commun 2:299. doi:10.1038/ncomms1298

Nagata T (1961) Rock magnetism, 2nd edn. Maruzen, Tokyo, p 350

O'Donovan JB, Facey D, O'Reilly W (1986) The magnetization process in titanomagnetite (Fe2.4Ti0.6O4) in the 1–30 μm particle size range. Geophys J R Astron Soc 87:897–916

Owens WH, Bamford D (1976) Magnetic, seismic, and other anisotropic properties of rock fabrics. Phil Trans R Soc Lond Ser A 283:55–68

Philpotts AR, Shi J, Brustman C (1998) Role of plagioclase crystal chains in differentiation of partly crystallized basaltic magma. Nature 395:343–346

Pike CR, Robert AP, Verosub KL (1999) Characterizing interactions in fine magnetic particle systems using first order reversal curves. J Appl Phys 85:6660–6667

Potter DK, Stephenson A (1988) Single-domain particles in rocks and magnetic fabric analysis. Geophys Res Lett 15:1097–1100

Rahman AA, Parry LG (1978) Titanomagnetites prepared at different oxidation conditions: hysteresis properties. Phys Earth Planet Inter 16:232–239

Raposo MI, Ernesto BM (1995) Anisotropy of magnetic susceptibility in the Ponta Grossa dike swarm (Brasil) and its relationship with magma flow direction. Phys Earth Planet Inter 87:183–196

Rochette P, Jenatton L, Dupuy C, Boudier F, Reuber I (1991) Diabase dikes emplacement in the Oman ophiolite: a magnetic fabric study with reference to geochemistry. In: Peters Tj, Nicolas A, Coleman RG (eds) Ophiolite genesis and evolution of the Oceanic lithosphere. Kluwer, Dordrecht, pp 55–82

Rochette P, Aubourg C, Perrin M (1999) Is this magnetic fabric normal? A review and case studies in volcanic formations. Tectonophysics 307:219–234

Stevenson CTE, Owens WH, Hutton DHW (2007) Flow lobes in granite: the determination of magma flow direction in the Trawenagh Bay Granite, northwestern Ireland, using anisotropy of magnetic susceptibility. GSA Bull 119:1368–1386

Symons DTA (1967) The magnetic and petrologic properties of a basalt column. Geophys J R Astron Soc 12:473–490

Urrutia-Fucugauchi J (1982) Magnetic anisotropy study of a columnar basalt from San Anton, Morelos, Mexico. Bull Volcanol 45:1–8

Vahle C, Kontny A (2005) The use of field dependence of AC susceptibility for the interpretation of magnetic mineralogy and magnetic fabrics in the HSDP-2 basalts, Hawaii. Earth Planet Sci Lett 238:110–129

Wright TL, Okamura RT (1977) Cooling and crystallization of the tholeiitic basalt, 1956 Makaopuhi lava lake, Hawaii. U.S. Geol Surv Prof Pap 1004:1–78